

Revealing the q^2 dependence in $b \rightarrow s\mu^+\mu^-$ baryonic decay modes

Ajay Kumar Yadav^{a,*}, Manas Kumar Mohapatra^{b,†} and Suchismita Sahoo^{a‡}

Department of Physics, Central University of Karnataka, Kalaburagi-585367, India ^a

School of Physics, University of Hyderabad, Hyderabad-500046, India ^b

Abstract

Measurements from the LHCb experiment and B factories have revealed several discrepancies in angular observables of rare semileptonic B decays involving the quark-level transition $b \rightarrow s\ell^+\ell^-$. In this work, we conduct a model-independent comparative analysis of the rare semileptonic decays of baryons Λ_b , Σ_b and Ξ_b , exploring various new physics scenarios. Our analysis includes predictions for branching ratios and angular observables, including forward-backward asymmetry, longitudinal polarization fractions, and lepton flavor universality ratios, both within the Standard Model and across six distinct new physics scenarios. Notably, we find that certain new physics scenarios significantly affect the observables in the $(\Lambda_b, \Sigma_b, \Xi_b) \rightarrow (\Lambda, \Sigma, \Xi)\mu^+\mu^-$ processes.

*Electronic address: yadavajaykumar286@gmail.com

†Electronic address: manasmohapatra12@gmail.com

‡Electronic address: suchismita8792@gmail.com

I. INTRODUCTION

The rare process induced by the flavor-changing neutral currents (FCNC) in the $b \rightarrow s\ell\ell$ transition serves as a critical testing ground for the Standard Model (SM) at loop level and is highly sensitive to new physics (NP) effects. Recent investigations into the $b \rightarrow s\mu^+\mu^-$ transitions have been particularly compelling due to anomalies reported by the LHCb and Belle II Collaborations[1–3]. Noteworthy among these anomalies are the ratios \mathcal{R}_K and \mathcal{R}_{K^*} [4], defined as

$$\mathcal{R}_{K^{(*)}} = \frac{\mathcal{BR}(B \rightarrow K^{(*)}\mu\mu)}{\mathcal{BR}(B \rightarrow K^{(*)}ee)}, \quad (1)$$

which are anticipated to be unity in the SM, embodying the principle of lepton flavor universality (LFU). These ratios are especially valuable due to their theoretical cleanliness, as hadronic uncertainties are expected to cancel out. Recent measurements from LHCb [5, 6] are consistent with the SM predictions for these ratios. However, other observables within $b \rightarrow s\ell\ell$ transitions, such as P'_5 and various branching fractions, display significant deviations from SM expectations. For example, deviations of 3.3σ in P'_5 have been reported by LHCb [7, 8] and ATLAS [9], while the branching ratio for $B_s \rightarrow \phi\mu^+\mu^-$ exhibits a 3.3σ deviation [10–12] in the q^2 range of $[1.1, 6.0]$ GeV 2 . Deviations of 1.4σ and 1.5σ have also been observed in the measurements of $\mathcal{R}_{K_S^0}$ and $\mathcal{R}_{K^{*+}}$ [13], respectively. Moreover, other observables such as forward-backward asymmetries, longitudinal polarization asymmetries, CP-averaged observables, and CP asymmetries in $B \rightarrow K^{(*)}\mu^+\mu^-$ decays across various q^2 intervals show deviations from SM predictions [14–21]. These discrepancies could potentially be due to new physics beyond the SM (BSM), a lack of comprehensive understanding of hadronic uncertainties, or limitations in the analysis of experimental data. Although the potential for BSM effects is intriguing, it is crucial to first enhance the theoretical framework addressing the substantial hadronic contributions in rare $b \rightarrow s$ transitions.

Exploring additional related decay channels could provide valuable insights complementary to the well-studied mesonic decays, thereby deepening our understanding of the anomalies observed in B -meson decays. While the focus in B -factory experiments has predominantly been on meson decays, the theoretical exploration of semileptonic baryon decays $B_1 \rightarrow B_2 l^+l^-$ is particularly noteworthy for several reasons:

- At the scale of quark-level transitions, the treatment of semileptonic baryon decays is considered to be analogous to that of mesons.

- Holds the potential to enhance our current understanding of the helicity structure within the underlying Hamiltonian [22].
- The spin of baryons influences certain kinematic observables, resulting in a greater number of degrees of freedom in the baryon bound states compared to mesons.

In this context, baryonic decay modes involving the $b \rightarrow s\ell^+\ell^-$ quark-level transition have garnered significant attention, prompting extensive theoretical investigation into processes such as $\Lambda_b \rightarrow \Lambda\mu^+\mu^-$, $\Sigma_b \rightarrow \Sigma\mu^+\mu^-$, and $\Xi_b \rightarrow \Xi\mu^+\mu^-$. Experimentally, the first observation of the rare baryonic $\Lambda_b \rightarrow \Lambda\mu^+\mu^-$ decay was reported by the CDF Collaboration [23], and more recently, this decay has also been investigated by the LHCb experiment [24, 25]. On the other hand, the experimental searches for the decays $\Sigma_b \rightarrow \Sigma\mu^+\mu^-$, and $\Xi_b \rightarrow \Xi\mu^+\mu^-$ are also viable at experiments like LHCb and/or Belle II [26, 27]. In this context, theoretical predictions are crucial for guiding these experimental efforts. Many theoretical analyses have been conducted to explore these decay processes in detail [28–43], providing valuable insights into their underlying dynamics.

In this study, we explore the impact of a model-independent effective theory formalism on exclusive $b \rightarrow s\mu^+\mu^-$ baryonic decay channels. We examine the effects of new physics through vector and axial-vector operators, fitting the associated new physics couplings. Our analysis incorporates experimental measurements of branching fractions for leptonic $B_s \rightarrow \mu^+\mu^-$, and semileptonic $B \rightarrow (K^{(*)}, \phi)\mu^+\mu^-$ decays, focusing on key observables such as forward-backward asymmetry, longitudinal polarization asymmetry, lepton non-universal ratios, and form factor-independent observables [44]. Additionally, we provide predictions for baryonic decays $(\Lambda_b, \Sigma_b, \Xi_b) \rightarrow (\Lambda, \Sigma, \Xi)\mu^+\mu^-$, both within the SM and in the context of effective field theory with new (axial)vector operators, and discuss the implications of these new couplings.

This paper is organized as follows: Section II provides an overview of the effective Hamiltonian relevant to semileptonic decays involving $b \rightarrow s\ell^+\ell^-$ quark-level transitions and details the expressions for the angular observables in the $B_1 \rightarrow B_2\mu^+\mu^-$ process. Section III focuses on the numerical fitting of new (axial)vector Wilson coefficients within both one-dimensional and two-dimensional scenarios, and examines the impact of these newly fitted parameters on $b \rightarrow s\mu^+\mu^-$ mediated baryonic decay observables. Finally, Section IV presents a summary and conclusion of our findings.

II. THEORETICAL FRAMEWORK

A. Effective Hamiltonian

The baryonic decay $B_1 \rightarrow B_2 \ell^+ \ell^-$, where $B_1 = \Lambda_b, \Sigma_b, \Xi_b$ and $B_2 = \Lambda, \Sigma, \Xi$, arises from a flavor-changing neutral current (FCNC) transition, described by the SM effective Hamiltonian, similar to other $b \rightarrow s \ell^+ \ell^-$ decays, and can be expressed as [22]

$$\mathcal{H}_{\text{eff}} = \frac{-4G_F}{\sqrt{2}} V_{tb} V_{ts}^* \left[\sum_{i=1}^6 C_i(\mu) \mathcal{O}_i + C_7^{(\prime)} \frac{e}{16\pi^2} (\bar{s}\sigma_{\mu\nu}(m_s P_L + m_b P_R)b) F^{\mu\nu} + C_9^{(\prime)} \frac{\alpha_e}{4\pi} (\bar{s}\gamma^\mu P_L b) \bar{\ell}\gamma_\mu \ell + C_{10}^{(\prime)} \frac{\alpha_e}{4\pi} (\bar{s}\gamma^\mu P_L b) \bar{\ell}\gamma_\mu \gamma_5 \ell \right].$$

Here, G_F (α_e) represents the Fermi coupling (fine structure constant), and the CKM matrix elements are denoted by $V_{tb} V_{ts}^*$. The relevant four-fermion operators, $\mathcal{O}_i^{(\prime)}$ for $i = 7, 9, 10$, are explicitly defined as

$$\begin{aligned} \mathcal{O}_7 &= \frac{e}{16\pi^2} m_b (\bar{s}\sigma_{\mu\nu} P_R b) F^{\mu\nu}, & \mathcal{O}'_7 &= \frac{e}{16\pi^2} m_b (\bar{s}\sigma_{\mu\nu} P_L b) F^{\mu\nu}, \\ \mathcal{O}_9 &= \frac{e^2}{16\pi^2} (\bar{s}\gamma_\mu P_L b) (\bar{\mu}\gamma^\mu \mu), & \mathcal{O}'_9 &= \frac{e^2}{16\pi^2} (\bar{s}\gamma_\mu P_R b) (\bar{\mu}\gamma^\mu \mu), \\ \mathcal{O}_{10} &= \frac{e^2}{16\pi^2} (\bar{s}\gamma_\mu P_L b) (\bar{\mu}\gamma^\mu \gamma_5 \mu), & \mathcal{O}'_{10} &= \frac{e^2}{16\pi^2} (\bar{s}\gamma_\mu P_R b) (\bar{\mu}\gamma^\mu \gamma_5 \mu), \end{aligned}$$

where $P_{R,L} = \frac{1 \pm \gamma_5}{2}$ are the chirality projection operators, and the $C_i^{(\prime)}$'s are the corresponding Wilson coefficients [45]. The couplings $C_{i=1,\dots,6}$ correspond to the Wilson coefficients associated with current-current operators ($i = 1, 2$) and QCD penguin operators ($i = 3, \dots, 6$). The couplings C_7 , ($C_9^{(\prime)}$, $C_{10}^{(\prime)}$) pertain to radiative (electromagnetic) penguin operators. It is worth noting that the SM does not contribute to the primed Wilson coefficients. These operators only emerge in extensions of the SM.

B. Observables of $B_1 \rightarrow B_2 \ell^+ \ell^-$ decays

The angular distribution of the baryonic decay $B_1 \rightarrow B_2$ can be parameterized in terms of q^2 , θ_{B_2} , θ_l , and ϕ , where q^2 denotes the square of the invariant mass of the lepton pair, θ_{B_2} and θ_l are the helicity angles of the hadronic and leptonic subsystems, respectively, and ϕ is the azimuthal angle between the two planes. The four-fold angular distribution for the

$B_1 \rightarrow B_2 \ell^+ \ell^-$ process is expressed as [32, 33]

$$\frac{d^4\Gamma}{dq^2 d\cos\theta_l d\cos\theta_{B_2} d\phi} = \frac{3}{8\pi} \mathcal{K}(q^2, \cos\theta_l, \cos\theta_{B_2}, \phi), \quad (2)$$

where $\mathcal{K}(q^2, \cos\theta_l, \cos\theta_{B_2}, \phi)$, described in terms of angular coefficients (\mathcal{K}_i), is expressed as

$$\begin{aligned} \mathcal{K}(q^2, \cos\theta_l, \cos\theta_{B_2}, \phi) = & \mathcal{K}_{1ss} \sin^2\theta_l + \mathcal{K}_{1cc} \cos^2\theta_l + \mathcal{K}_{1c} \cos\theta_l + \\ & (\mathcal{K}_{2ss} \sin^2\theta_l + \mathcal{K}_{2cc} \cos^2\theta_l + \mathcal{K}_{2c} \cos\theta_l) \cos\theta_{B_2} + \\ & (\mathcal{K}_{3sc} \sin\theta_l \cos\theta_l + \mathcal{K}_{3s} \sin\theta_l) \sin\theta_{B_2} \cos\phi + \\ & (\mathcal{K}_{4sc} \sin\theta_l \cos\theta_l + \mathcal{K}_{4s} \sin\theta_l) \sin\theta_{B_2} \sin\phi. \end{aligned}$$

The detailed expressions for the angular coefficients are provided in Appendix A. From the differential decay distributions given in Eq. (2), one can construct the following observables:

☞ The differential decay rate with q^2 [32, 33]:

$$\frac{d\Gamma}{dq^2} = 2\mathcal{K}_{1ss} + \mathcal{K}_{1cc}. \quad (3)$$

☞ The lepton flavor universality violation observable:

$$\mathcal{R}_{B_2}(q^2) = \frac{d\Gamma/dq^2|_\mu}{d\Gamma/dq^2|_e}. \quad (4)$$

☞ The forward-backward asymmetry [33, 34]:

- Leptonic:

$$\mathcal{A}_{FB}^\ell = \frac{3}{2} \frac{\mathcal{K}_{1c}}{2\mathcal{K}_{1ss} + \mathcal{K}_{1cc}}, \quad (5)$$

- Leptonic - Hadronic:

$$\mathcal{A}_{FB}^{\ell, B_2} = \frac{3}{4} \frac{\mathcal{K}_{2c}}{2\mathcal{K}_{1ss} + \mathcal{K}_{1cc}}, \quad (6)$$

- Hadronic:

$$\mathcal{A}_{FB}^{B_2} = \frac{1}{2} \frac{2\mathcal{K}_{2ss} + \mathcal{K}_{2cc}}{2\mathcal{K}_{1ss} + \mathcal{K}_{1cc}}. \quad (7)$$

☞ The longitudinal polarization asymmetry [32–34]:

$$\mathcal{F}_L = \frac{2\mathcal{K}_{1ss} - \mathcal{K}_{1cc}}{2\mathcal{K}_{1ss} + \mathcal{K}_{1cc}}. \quad (8)$$

By definition, the transverse polarization fraction is $\mathcal{F}_T = 1 - \mathcal{F}_L$.

C. Inputs

Prior to commencing our analysis, we outline the key input parameters utilized in the numerical computation. For the masses of the leptons, mesons and baryons, the lifetime parameters, and the CKM matrix elements, we use Ref. [46]. For the baryonic form factors, we utilize Lattice QCD calculations for the $\Lambda_b \rightarrow \Lambda$ transition, as detailed in Ref.[34]. For the $\Sigma_b \rightarrow \Sigma$ and $\Xi_b \rightarrow \Xi$ transitions, we adopt the Light-Cone QCD Sum Rules method, following Refs. [28, 47] and [29], respectively. Further details on the form factors are provided in Appendix B.

III. NEW PHYSICS SENSITIVITY

A. Constraint on new physics coupling(s)

To investigate the observed discrepancies in $b \rightarrow s\mu^+\mu^-$ transitions, we employ a model-independent framework for a thorough data analysis. We focus on observables in $b \rightarrow s\mu^+\mu^-$ decays that exhibit deviations from Standard Model predictions. Particular emphasis is placed on scenarios involving the vector and axial-vector Wilson coefficients $C_9^{(\prime)\text{NP}}$ and $C_{10}^{(\prime)\text{NP}}$, which may indicate contributions from new physics. In this context, we utilize the new physics coupling parameters associated with the most favorable p-values, as computed in our previous work [44]. Specifically, we examine six scenarios: two one dimensional and four two dimensional that yield the best p-values. Detailed information is provided in Table I.

TABLE I: Best-fit values [1σ], pull and p-value(%) for 1D and 2D new physics scenarios.

Scenario	Coefficient	Best fit value [1σ]	Pull	p-value (%)
S - A	C_9^{NP}	$-1.227 [-^{0.959}_{-1.363}]$	4.665	46.0
S - B	$C_9^{\text{NP}} = -C_{10}^{\text{NP}}$	$-0.971 [-^{0.757}_{-1.161}]$	4.921	53.0
S - C	$(C_9^{\text{NP}}, C_{10}^{\text{NP}})$	$(-1.398[-^{1.219}_{-1.578}], 0.694[^{0.855}_{-0.480}])$	5.961	67.0
S - D	$(C_9^{\text{NP}}, C_{10}^{\prime\text{NP}})$	$(-1.269[-^{1.079}_{-1.454}], -0.306[-^{0.158}_{-0.390}])$	5.239	53.0
S - E	$(C_9^{\text{NP}} = C_9^{\prime\text{NP}}, C_{10}^{\text{NP}} = -C_{10}^{\prime\text{NP}})$	$(-1.121[-^{0.911}_{-1.330}], 0.302[^{0.365}_{-0.198}])$	5.174	51.0
S - F	$(C_9^{\text{NP}} = -C_{10}^{\text{NP}}, C_9^{\prime\text{NP}} = C_{10}^{\prime\text{NP}})$	$(-0.986[-^{0.783}_{-1.189}], 0.108[^{0.232}_{-0.015}])$	5.412	53.0

B. Results and Discussion

We have conducted a thorough theoretical and numerical analysis, resulting in several key insights. Our findings are examined across six distinct scenarios: **S - A**, **S - B**, **S - C**, **S - D**, **S - E** and **S - F**. We will provide a detailed discussion of these results and clarify the color coding used in the plots to facilitate a comprehensive understanding.

Using the 1σ range of new coefficients for all scenarios, we present the branching ratios and angular observables in five q^2 bins: $q^2 \in [0.1, 0.98] \text{ GeV}^2$, $q^2 \in [1.1, 2.5] \text{ GeV}^2$, $q^2 \in [2.5, 4] \text{ GeV}^2$, $q^2 \in [4, 6] \text{ GeV}^2$, and the full low q^2 region $q^2 \in [1, 6] \text{ GeV}^2$. Fig.1 displays the branching ratios for the semileptonic baryonic decay processes $\Lambda_b \rightarrow \Lambda\mu^+\mu^-$ (left), $\Sigma_b \rightarrow \Sigma\mu^+\mu^-$ (middle) and $\Xi_b \rightarrow \Xi\mu^+\mu^-$ (right) for the q^2 bins $[0.1, 0.98]$ (top), $[1.1, 2.5]$ (second from top), $[2.5, 4]$ (second from bottom) and $[4, 6]$ (bottom). The lepton non-universality (LNU) parameters \mathcal{R}_Λ (left), \mathcal{R}_Σ (middle) and \mathcal{R}_Ξ (right) are illustrated in Fig. 2 for the four q^2 bins. Additionally, Figs. 3, 4 and 5 showcase the leptonic, leptonic-hadronic, and hadronic forward backward asymmetries, respectively, for all three channels across the discussed q^2 bins. The longitudinal polarization asymmetries for the semileptonic decays of Λ_b , Σ_b and Ξ_b are depicted in Fig.6. Figures 7 and 8 provide the predicted 1σ ranges for various observables of $\Lambda_b \rightarrow \Lambda$ (left), $\Sigma_b \rightarrow \Sigma$ (middle) and $\Xi_b \rightarrow \Xi$ (right) within the low q^2 region $[1, 6] \text{ GeV}^2$. In particular, Fig. 7 includes the branching ratio (top), LNU parameters (middle), and longitudinal polarization asymmetry (bottom). Meanwhile, Fig. 8 features the leptonic (top), leptonic-hadronic (middle), and hadronic (bottom) forward-backward asymmetries. In all figures, the Cyan band denotes the SM contribution, with the band indicating the 1σ theoretical uncertainties. For the NP scenarios, the color coding is as follows: Orange for **S - A**, Purple for **S - B**, Brown for **S - C**, Magenta for **S - D**, Blue for **S - E**, Green for **S - F**. The color bands in these scenarios represent the predicted 1σ range of the observables based on the 1σ range of the new coefficients. The estimated binwise numerical values for the branching ratios of $B_1 \rightarrow B_2\mu^+\mu^-$ baryonic decays, both within the SM and across all six NP scenarios, are presented in Table II. Binwise predictions for the LNU parameters are provided in Table III for all q^2 bins. Tables VII and VIII display the numerical results for longitudinal and transverse polarization, respectively. The estimations for the leptonic, leptonic-hadronic, and hadronic forward backward asymmetries of the baryonic decay modes across five q^2 bins are shown in Tables IV, V and VI.

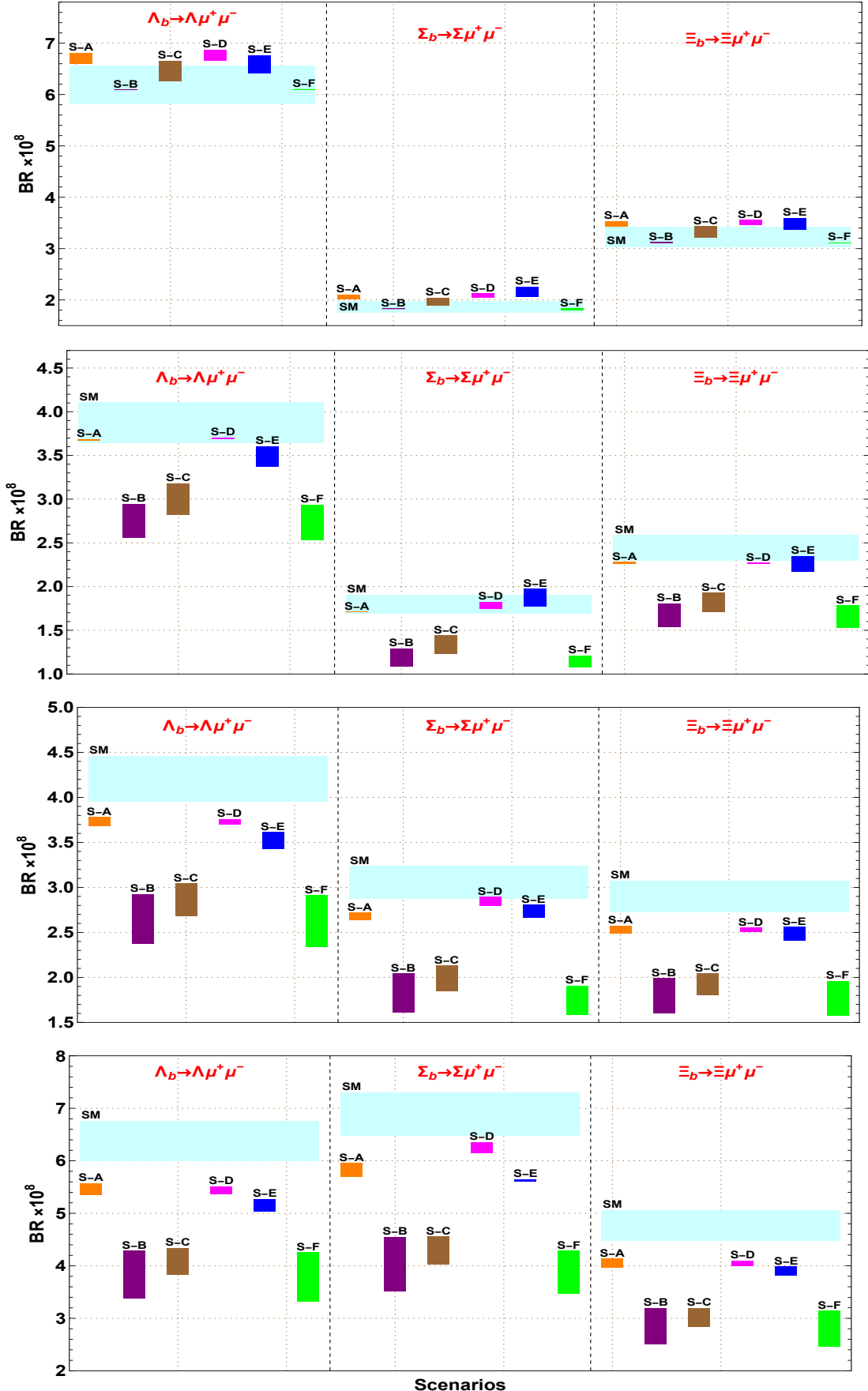


FIG. 1: $\mathcal{BR}(\Lambda_b \rightarrow \Lambda\mu\mu)$ (left), $\mathcal{BR}(\Sigma_b \rightarrow \Sigma\mu\mu)$ (middle) and $\mathcal{BR}(\Xi_b \rightarrow \Xi\mu\mu)$ (right) are shown across q^2 bins: $q^2 \in [0.1, 0.98]$ (top), $q^2 \in [1.1, 2.5]$ (second from top), $q^2 \in [2.5, 4.0]$ (second from bottom), $q^2 \in [4.0, 6.0]$ (bottom). The bands indicate 1σ uncertainty.

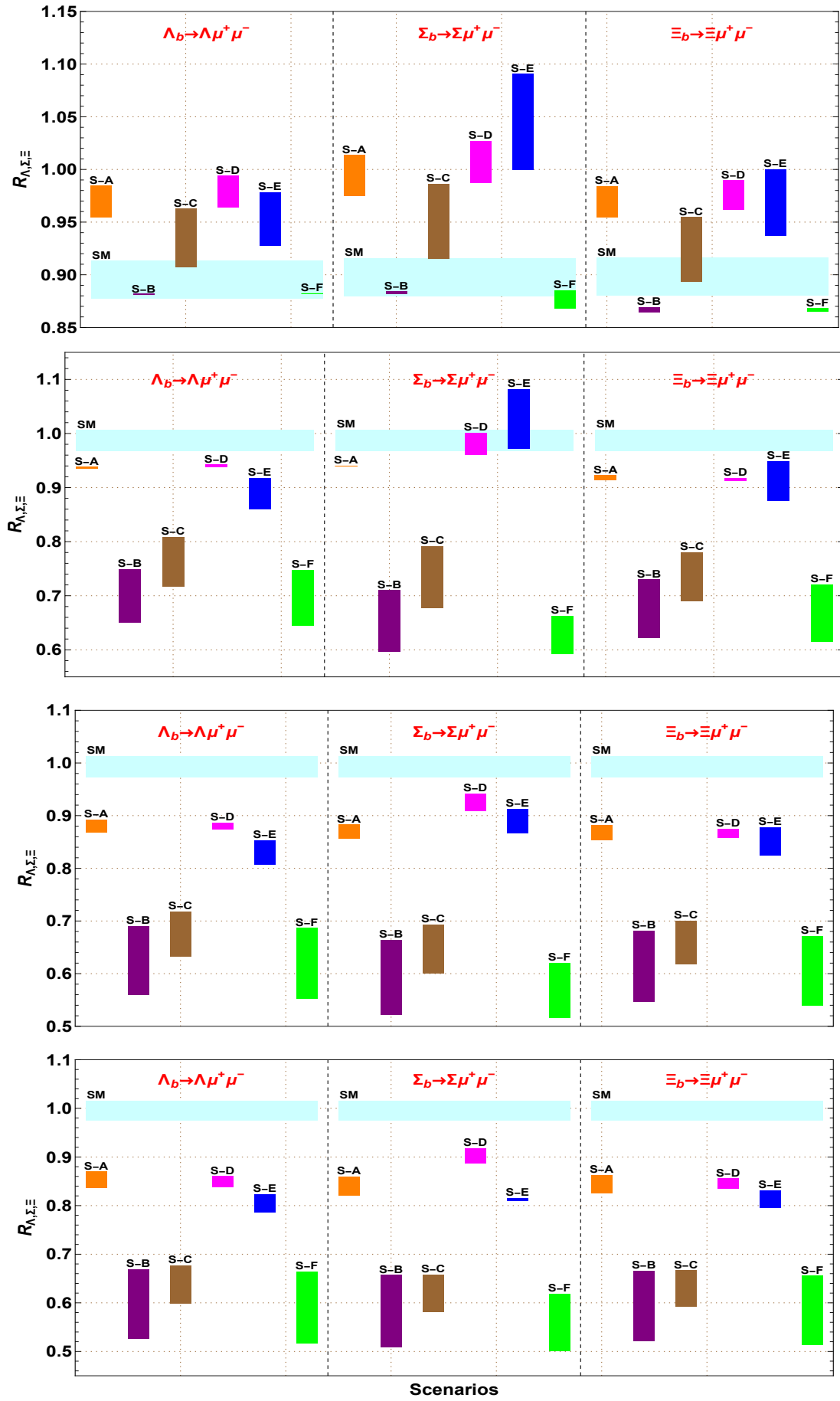


FIG. 2: Same as Fig. 1, illustrating the observables \mathcal{R}_Λ (left), \mathcal{R}_Σ (middle), and \mathcal{R}_Ξ (right).

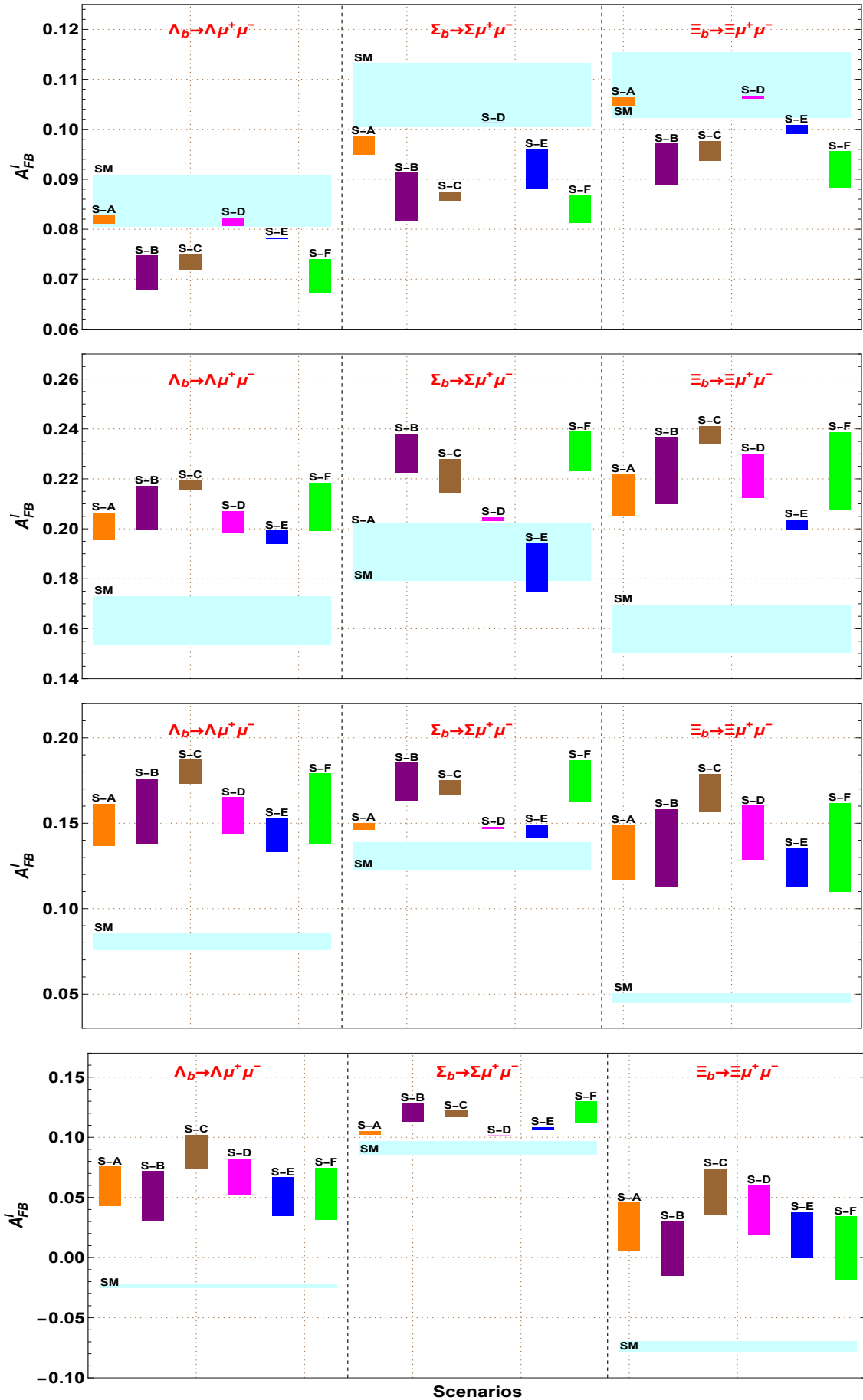


FIG. 3: Same as Fig. 1, focusing the observables $\mathcal{A}_{FB}^\ell(\Lambda_b \rightarrow \Lambda \mu \mu)$ (left), $\mathcal{A}_{FB}^\ell(\Sigma_b \rightarrow \Sigma \mu \mu)$ (middle) and $\mathcal{A}_{FB}^\ell(\Xi_b \rightarrow \Xi \mu \mu)$ (right).

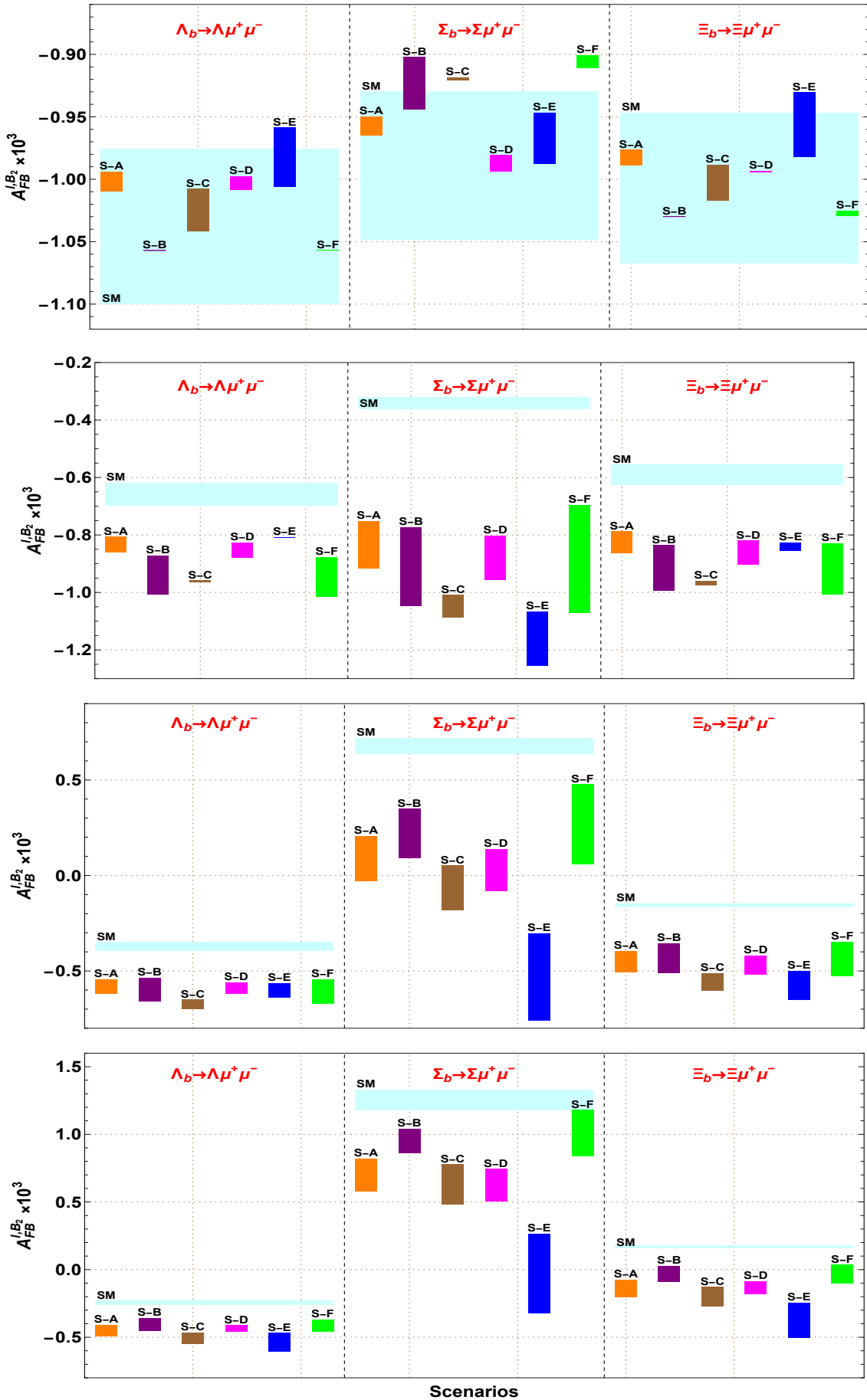


FIG. 4: Same as Fig. 1, displaying the observables $\mathcal{A}_{FB}^{\ell, B_2}(\Lambda_b \rightarrow \Lambda \mu \mu)$ (left),
 $\mathcal{A}_{FB}^{\ell, B_2}(\Sigma_b \rightarrow \Sigma \mu \mu)$ (middle) and $\mathcal{A}_{FB}^{\ell, B_2}(\Xi_b \rightarrow \Xi \mu \mu)$ (right).

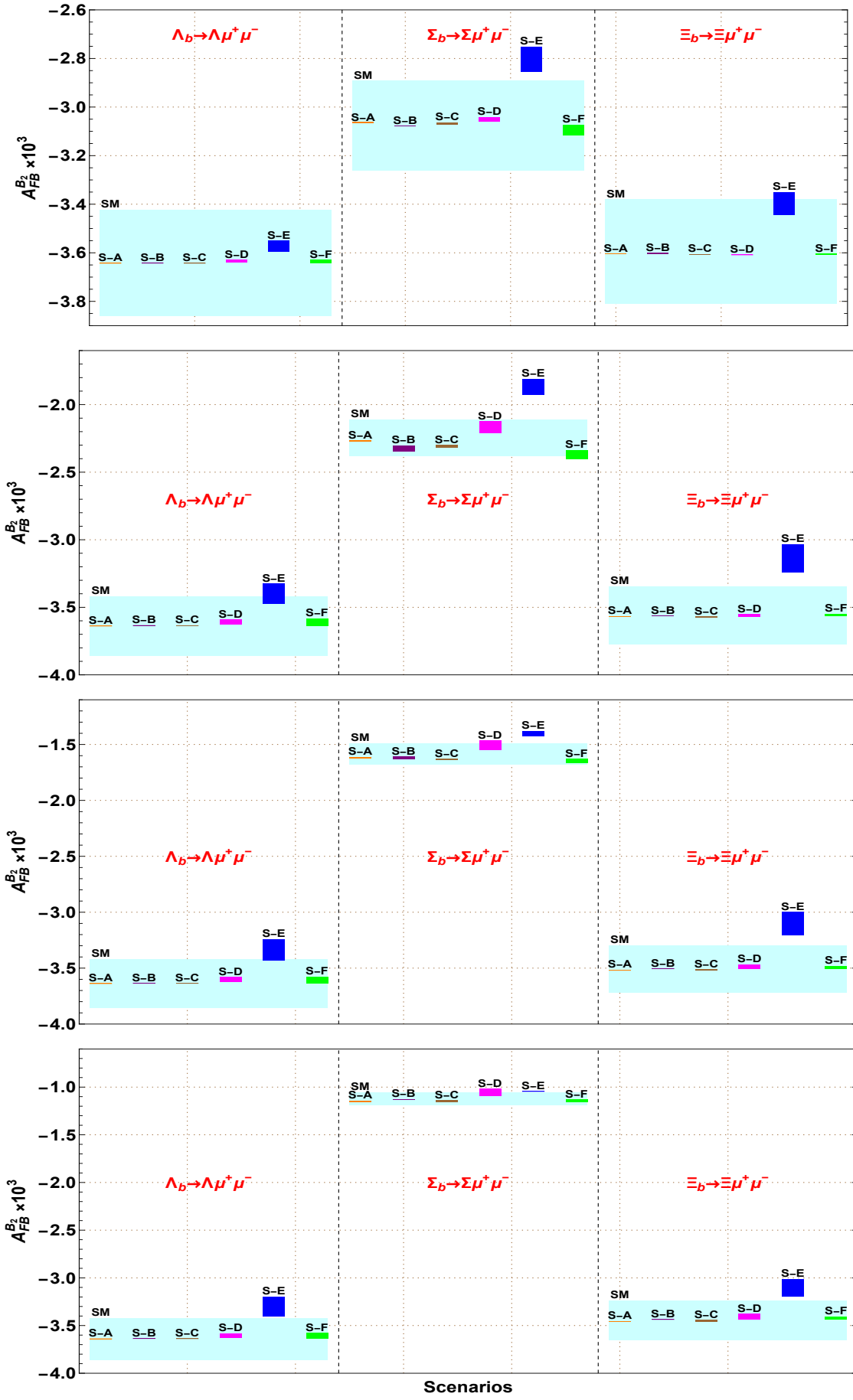


FIG. 5: Same as Fig. 1, emphasizing the observables $\mathcal{A}_{FB}^{B_2}(\Lambda_b \rightarrow \Lambda \mu \mu)$ (left), $\mathcal{A}_{FB}^{B_2}(\Sigma_b \rightarrow \Sigma \mu \mu)$ (middle) and $\mathcal{A}_{FB}^{B_2}(\Xi_b \rightarrow \Xi \mu \mu)$ (right).

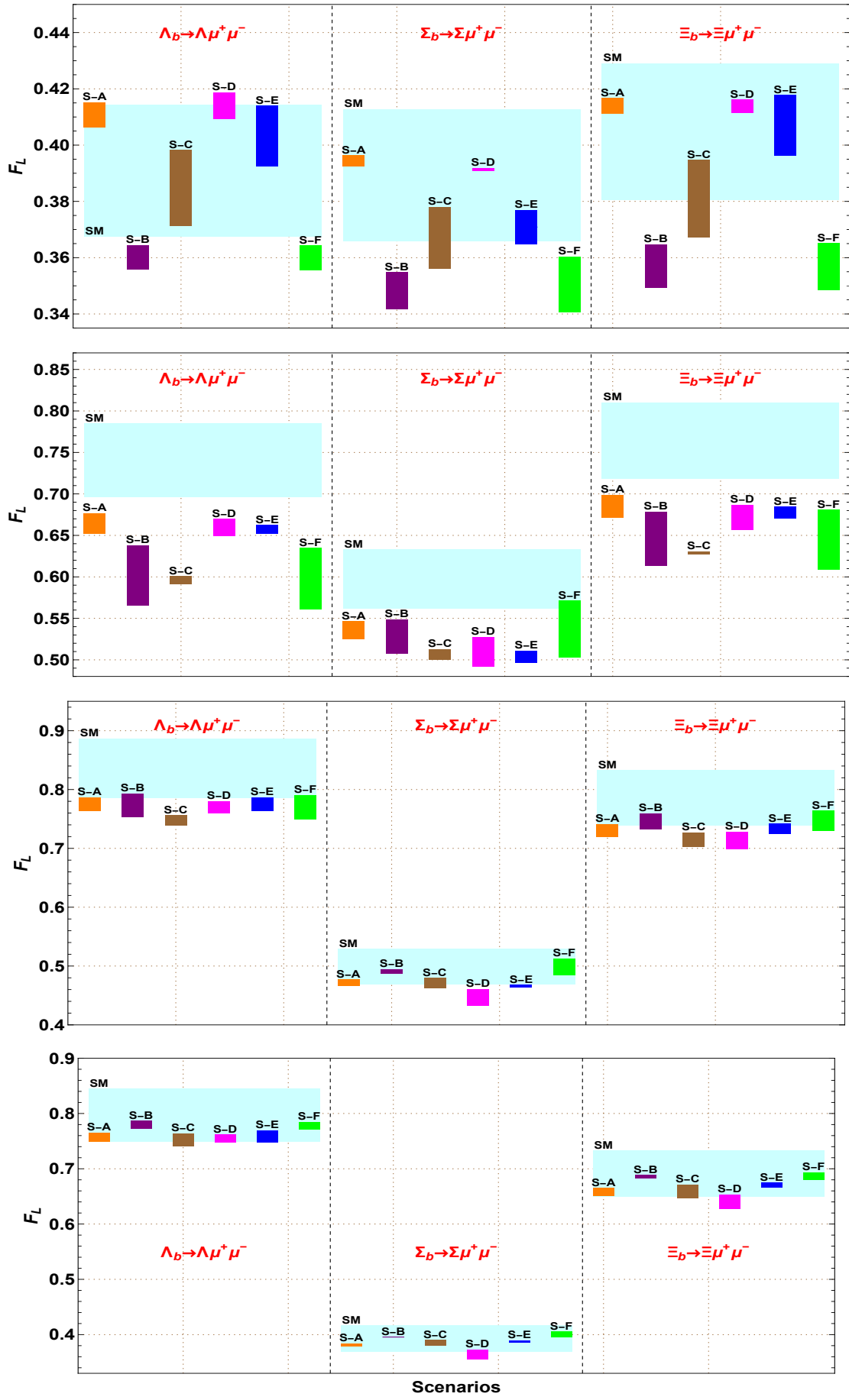


FIG. 6: Same as Fig. 1, featuring the observables $\mathcal{F}_L(\Lambda_b \rightarrow \Lambda \mu \mu)$ (left), $\mathcal{F}_L(\Sigma_b \rightarrow \Sigma \mu \mu)$ (middle) and $\mathcal{F}_L(\Xi_b \rightarrow \Xi \mu \mu)$ (right).

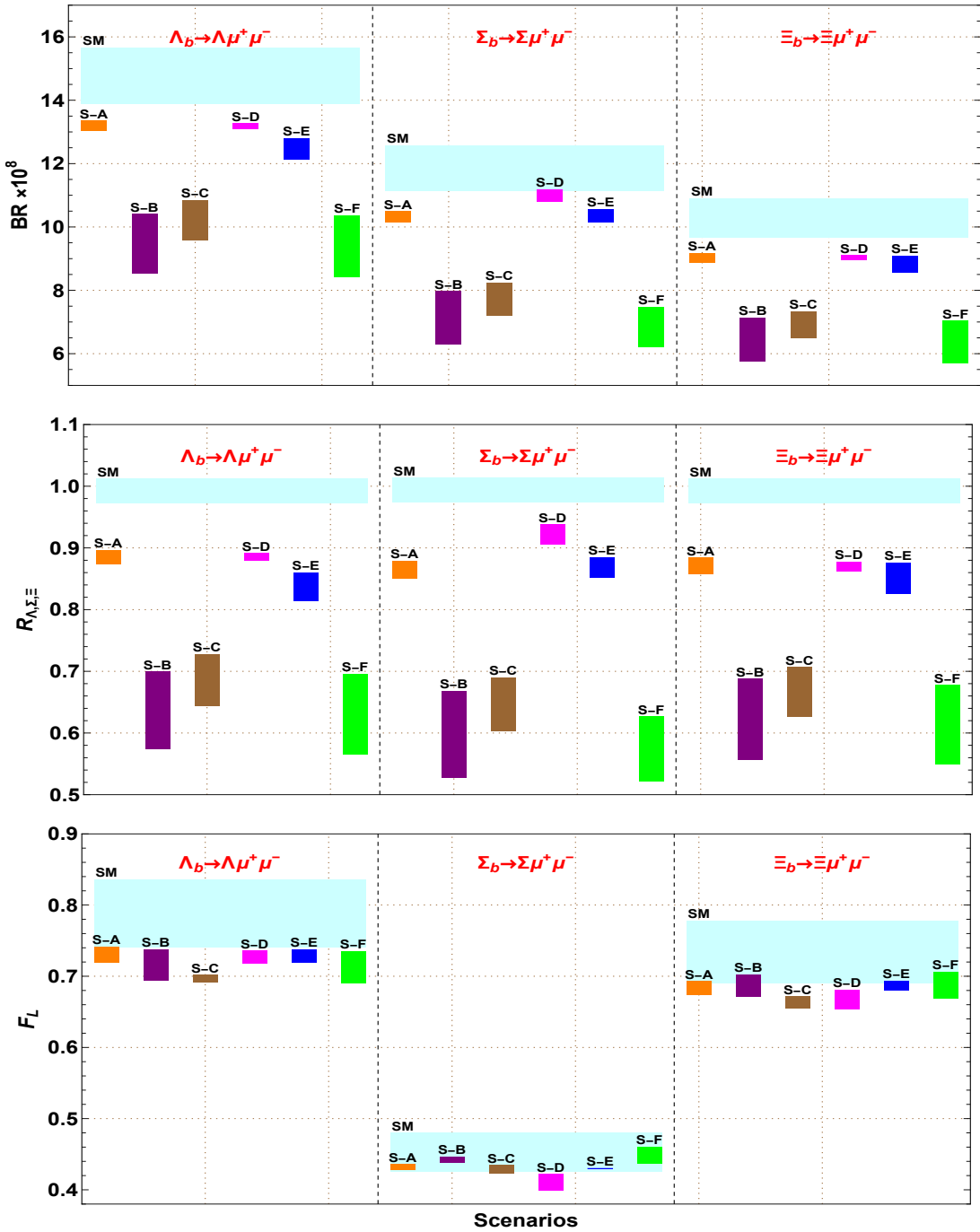


FIG. 7: Same as Fig. 1, showcasing the observables: branching ratio (top), LNU parameter (middle), longitudinal polarisation asymmetry (bottom) in the low q^2 region [1, 6] GeV 2 .

- The branching ratios for the $\Lambda_b \rightarrow \Lambda \mu^+ \mu^-$ decay mode within the SM across the five q^2 bins are $(6.189, 3.875, 4.208, 6.378, 14.77) \times 10^{-8}$ (Table II). In the $q^2 \in [0.1, 0.98]$ GeV 2 bin, the central values of the branching fractions from all six new physics scenarios are consistent with those of the SM. However, for the remaining q^2 bins, scenarios B ($C_9^{\text{NP}} = -C_{10}^{\text{NP}}$), C ($C_9^{\text{NP}}, C_{10}^{\text{NP}}$) and F ($C_9^{\text{NP}} = -C_{10}^{\text{NP}}, C'_9^{\text{NP}} = -C'_{10}^{\text{NP}}$) yield significantly

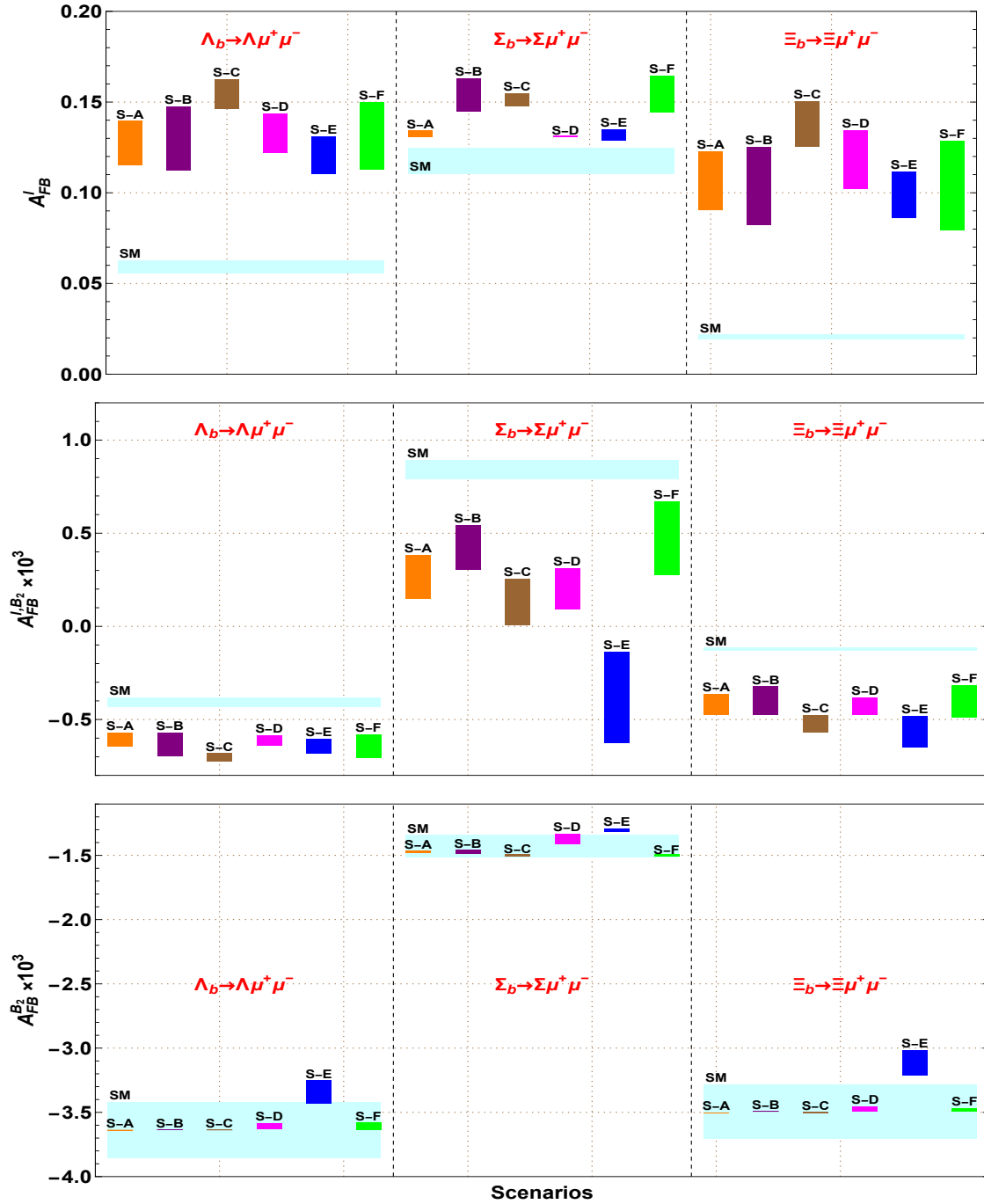


FIG. 8: Same as Fig. 1, presenting the observables: \mathcal{A}_{FB}^μ (top), $\mathcal{A}_{FB}^{\mu, B_2}$ (middle) and $\mathcal{A}_{FB}^{B_2}$ (bottom) in the low $q^2 \in [1, 6]$ GeV 2 region.

smaller central values compared to scenarios A, D, and E. This pattern is also observed when comparing these results with the branching ratios of $\Sigma_b(\Xi_b) \rightarrow \Sigma(\Xi)\mu^+\mu^-$ across all q^2 bins. In summary, for all three semileptonic baryonic decays, there is no deviation from the SM in the $q^2 \in [0.1, 0.98]$ bin; however, significant deviations from the SM are observed in the remaining four bins for scenarios B, C, and F.

TABLE II: Numerical predictions for the branching ratios of $(\Lambda_b, \Sigma_b, \Xi_b) \rightarrow (\Lambda, \Sigma, \Xi)\mu^+\mu^-$ decay modes in different q^2 bins within the SM and across six new physics scenarios.

Bins	SM	S - A	S - B	S - C	S - D	S - E	S - F
$\mathcal{BR}(\Lambda_b \rightarrow \Lambda\mu^+\mu^-) \times 10^8$							
$q_{[0.1,0.98]}^2$	6.189	6.735	6.089	6.445	6.767	6.572	6.092
$q_{[1.1,2.5]}^2$	3.875	3.671	2.729	2.965	3.690	3.458	2.721
$q_{[2.5,4]}^2$	4.208	3.710	2.621	2.820	3.725	3.481	2.608
$q_{[4,6]}^2$	6.378	5.420	3.784	4.024	5.434	5.100	3.760
$q_{[1,6]}^2$	14.77	13.11	9.38	10.08	13.17	12.34	9.336
$\mathcal{BR}(\Sigma_b \rightarrow \Sigma\mu^+\mu^-) \times 10^8$							
$q_{[0.1,0.98]}^2$	1.859	2.071	1.826	1.963	2.086	2.158	1.813
$q_{[1.1,2.5]}^2$	1.799	1.710	1.179	1.320	1.795	1.856	1.136
$q_{[2.5,4]}^2$	3.054	2.658	1.802	1.958	2.862	2.711	1.735
$q_{[4,6]}^2$	6.896	5.771	3.984	4.224	6.230	5.582	3.850
$q_{[1,6]}^2$	11.86	10.25	7.05	7.596	11.07	10.28	6.803
$\mathcal{BR}(\Xi_b \rightarrow \Xi\mu^+\mu^-) \times 10^8$							
$q_{[0.1,0.98]}^2$	3.231	3.503	3.115	3.313	3.508	3.474	3.112
$q_{[1.1,2.5]}^2$	2.440	2.263	1.658	1.797	2.261	2.237	1.645
$q_{[2.5,4]}^2$	2.899	2.517	1.774	1.898	2.525	2.458	1.755
$q_{[4,6]}^2$	4.772	4.012	2.813	2.972	4.051	3.859	2.782
$q_{[1,6]}^2$	10.29	8.973	6.385	6.819	9.018	8.733	6.321

- In the $q^2 \in [0.1, 0.98]$ bin, scenarios A, D, and E significantly impact the lepton non-universality parameters \mathcal{R}_Λ , \mathcal{R}_Σ , \mathcal{R}_Ξ . Conversely, scenarios B and F yield results consistent with the Standard Model, while scenario C shows only a marginal effect. For the remaining q^2 bins, scenarios B, C, and F exhibit comparatively larger contributions to all three lepton non-universality parameters. In the Standard Model and across all bins, \mathcal{R}_{B_2} is found to be less than one, whereas \mathcal{R}_Σ is slightly greater than one in scenarios A, D, and E for the first q^2 bin ($[0.1, 0.98]$) and in scenario E for the second q^2 bin ($[1.1, 2.5]$).

TABLE III: Same as Table II, presenting the lepton non-universality parameters for $B_1 \rightarrow B_2 \mu^+ \mu^-$ decay modes.

Bins	SM	S - A	S - B	S - C	S - D	S - E	S - F
\mathcal{R}_Λ							
$q_{[0.1,0.98]}^2$	0.895	0.974	0.881	0.932	0.979	0.951	0.881
$q_{[1.1,2.5]}^2$	0.987	0.935	0.695	0.755	0.94	0.88	0.693
$q_{[2.5,4]}^2$	0.993	0.876	0.619	0.666	0.879	0.822	0.615
$q_{[4,6]}^2$	0.996	0.846	0.591	0.628	0.848	0.796	0.587
$q_{[1,6]}^2$	0.992	0.881	0.63	0.677	0.884	0.829	0.627
\mathcal{R}_Σ							
$q_{[0.1,0.98]}^2$	0.898	1.0002	0.882	0.948	1.007	1.042	0.875
$q_{[1.1,2.5]}^2$	0.987	0.939	0.647	0.724	0.985	1.02	0.623
$q_{[2.5,4]}^2$	0.993	0.864	0.586	0.637	0.931	0.882	0.564
$q_{[4,6]}^2$	0.996	0.833	0.575	0.61	0.91	0.81	0.556
$q_{[1,6]}^2$	0.993	0.859	0.591	0.636	0.928	0.861	0.57
\mathcal{R}_Ξ							
$q_{[0.1,0.98]}^2$	0.898	0.974	0.866	0.921	0.975	0.966	0.865
$q_{[1.1,2.5]}^2$	0.987	0.915	0.670	0.727	0.914	0.904	0.665
$q_{[2.5,4]}^2$	0.993	0.862	0.608	0.65	0.865	0.842	0.601
$q_{[4,6]}^2$	0.995	0.837	0.587	0.62	0.845	0.805	0.58
$q_{[1,6]}^2$	0.992	0.865	0.616	0.657	0.869	0.842	0.609

- For the leptonic forward backward asymmetry of the $\Lambda_b \rightarrow \Lambda \mu^+ \mu^-$ decay mode, shifts in values compared to the SM are observed across all q^2 bins. Specifically, in the range $q^2 \in [0.1, 0.98]$, a decrease in asymmetry is seen for scenarios B, C, and F, while scenarios A, D, and E yield results that are nearly consistent with the SM. In the other q^2 bins, the shifts generally show an increasing trend. In contrast, the contributions of new physics scenarios to the forward backward asymmetry \mathcal{A}_{FB}^μ for $\Sigma_b \rightarrow \Sigma \mu^+ \mu^-$ are relatively modest across all q^2 bins. However, for $\Xi_b \rightarrow \Xi \mu^+ \mu^-$, the predicted \mathcal{A}_{FB}^μ values are significantly higher compared to the Λ_b and Σ_b decays, with the dominant

TABLE IV: Similar to Table II, showing the leptonic forward backward asymmetry observable of $B_1 \rightarrow B_2 \mu^+ \mu^-$ decay modes.

Bins	SM	S - A	S - B	S - C	S - D	S - E	S - F
$\mathcal{A}_{FB}^\mu(\Lambda_b \rightarrow \Lambda \mu^+ \mu^-)$							
$q_{[0,1,0.98]}^2$	0.086	0.0818	0.071	0.073	0.082	0.078	0.071
$q_{[1,1,2.5]}^2$	0.163	0.203	0.21	0.219	0.203	0.197	0.21
$q_{[2,5,4]}^2$	0.081	0.153	0.157	0.181	0.155	0.144	0.158
$q_{[4,6]}^2$	-0.024	0.064	0.051	0.089	0.067	0.05	0.052
$q_{[1,6]}^2$	0.059	0.131	0.131	0.156	0.133	0.121	0.131
$\mathcal{A}_{FB}^\mu(\Sigma_b \rightarrow \Sigma \mu^+ \mu^-)$							
$q_{[0,1,0.98]}^2$	0.107	0.096	0.086	0.086	0.102	0.092	0.084
$q_{[1,1,2.5]}^2$	0.191	0.201	0.231	0.223	0.204	0.186	0.232
$q_{[2,5,4]}^2$	0.131	0.149	0.174	0.172	0.147	0.146	0.175
$q_{[4,6]}^2$	0.091	0.104	0.121	0.12	0.101	0.108	0.121
$q_{[1,6]}^2$	0.118	0.133	0.154	0.153	0.131	0.133	0.155
$\mathcal{A}_{FB}^\mu(\Xi_b \rightarrow \Xi \mu^+ \mu^-)$							
$q_{[0,1,0.98]}^2$	0.109	0.105	0.093	0.095	0.107	0.1	0.092
$q_{[1,1,2.5]}^2$	0.16	0.217	0.224	0.239	0.222	0.203	0.224
$q_{[2,5,4]}^2$	0.0476	0.138	0.136	0.169	0.145	0.125	0.135
$q_{[4,6]}^2$	-0.074	0.032	0.007	0.055	0.04	0.018	0.006
$q_{[1,6]}^2$	0.021	0.112	0.104	0.139	0.119	0.099	0.103

contribution coming from scenario C, except in the first q^2 bin.

For the leptonic-hadronic forward backward asymmetry of all the semileptonic baryonic decay modes, the predictions from the six new physics scenarios generally fall within the SM's 1σ error band. However, there is a marginal shift for scenarios C and F in the $\mathcal{A}_{FB}^{\mu,\Sigma}$ for the $q^2 \in [0.1, 0.98]$ bin. In the remaining q^2 bins, all the new physics scenarios tend to predict larger negative values for $\mathcal{A}_{FB}^{\mu,B_2}$ compared to the SM. Notably, the impact of new physics is more pronounced for the $\Sigma_b \rightarrow \Sigma \mu^+ \mu^-$ decay, with scenario E predicting particularly large negative values for $\mathcal{A}_{FB}^{\mu,\Sigma}$ relative to the

TABLE V: In the same format as Table II, depicting the leptonic hadronic forward backward asymmetry observable of $B_1 \rightarrow B_2 \mu^+ \mu^-$ decays.

Bins	SM	S - A	S - B	S - C	S - D	S - E	S - F
$\mathcal{A}_{FB}^{\mu,\Lambda}(\Lambda_b \rightarrow \Lambda \mu^+ \mu^-) \times 10^3$							
$q_{[0,1,0.98]}^2$	-1.038	-0.999	-1.058	-1.026	-1.004	-0.984	-1.058
$q_{[1,1,2.5]}^2$	-0.659	-0.844	-0.940	-0.968	-0.854	-0.814	-0.946
$q_{[2.5,4]}^2$	-0.373	-0.593	-0.597	-0.679	-0.587	-0.605	-0.602
$q_{[4,6]}^2$	-0.247	-0.462	-0.403	-0.508	-0.433	-0.538	-0.408
$q_{[1,6]}^2$	-0.405	-0.620	-0.634	-0.709	-0.609	-0.646	-0.639
$\mathcal{A}_{FB}^{\mu,\Sigma}(\Sigma_b \rightarrow \Sigma \mu^+ \mu^-) \times 10^3$							
$q_{[0,1,0.98]}^2$	-0.989	-0.955	-0.923	-0.919	-0.992	-0.969	-0.908
$q_{[1,1,2.5]}^2$	-0.342	-0.861	-0.915	-1.056	-0.883	-1.175	-0.881
$q_{[2.5,4]}^2$	0.679	0.051	0.220	-0.069	0.029	-0.542	0.284
$q_{[4,6]}^2$	1.257	0.664	0.955	0.632	0.621	-0.032	1.028
$q_{[1,6]}^2$	0.843	0.228	0.425	0.131	0.203	-0.391	0.489
$\mathcal{A}_{FB}^{\mu,\Xi}(\Xi_b \rightarrow \Xi \mu^+ \mu^-) \times 10^3$							
$q_{[0,1,0.98]}^2$	-1.007	-0.981	-1.031	-1.004	0.996	-0.958	-1.029
$q_{[1,1,2.5]}^2$	-0.591	-0.839	-0.917	-0.973	-0.864	-0.847	-0.916
$q_{[2.5,4]}^2$	-0.157	-0.468	-0.433	-0.563	-0.466	-0.580	-0.430
$q_{[4,6]}^2$	0.168	-0.158	-0.032	-0.201	-0.129	-0.379	-0.027
$q_{[1,6]}^2$	-0.123	-0.435	-0.399	-0.527	-0.427	-0.569	-0.396

SM.

All predictions for the hadronic forward-backward asymmetry across the three baryonic decay channels, for all new physics scenarios and q^2 bins, fall within the SM error band. However, there is a marginal deviation observed in the $\mathcal{A}_{FB}^{\mu,\Sigma}$ measurements in the first and second q^2 bins due to the presence of scenario E.

- Examining the predictions for longitudinal polarization asymmetry in the $q^2 \in [0.1, 0.98]$ bin, we observe results that are almost consistent with the SM, except for scenarios B and F. In the $q^2 \in [1.1, 2.5]$ bin, there is a marginal deviation from the

TABLE VI: Similar to Table II, displaying the hadronic forward backward asymmetry observable of $B_1 \rightarrow B_2 \mu^+ \mu^-$ decay modes.

Bins	SM	S - A	S - B	S - C	S - D	S - E	S - F
$\mathcal{A}_{FB}^\Lambda(\Lambda_b \rightarrow \Lambda \mu^+ \mu^-) \times 10^3$							
$q_{[0,1,0.98]}^2$	-3.642	-3.643	-3.642	-3.643	-3.634	-3.574	-3.638
$q_{[1,1,2.5]}^2$	-3.637	-3.638	-3.635	-3.637	-3.607	-3.405	-3.617
$q_{[2.5,4]}^2$	-3.637	-3.638	-3.634	-3.636	-3.600	-3.340	-3.614
$q_{[4,6]}^2$	-3.639	-3.640	-3.636	-3.640	-3.602	-3.305	-3.617
$q_{[1,6]}^2$	-3.638	-3.639	-3.635	-3.637	-3.604	-3.347	-3.616
$\mathcal{A}_{FB}^\Sigma(\Sigma_b \rightarrow \Sigma \mu^+ \mu^-) \times 10^3$							
$q_{[0,1,0.98]}^2$	-3.078	-3.062	-3.077	-3.067	-3.049	-2.802	-3.096
$q_{[1,1,2.5]}^2$	-2.246	-2.269	-2.324	-2.312	-2.156	-1.866	-2.382
$q_{[2.5,4]}^2$	-1.584	-1.620	-1.620	-1.637	-1.497	-1.399	-1.656
$q_{[4,6]}^2$	-1.123	-1.151	-1.129	-1.150	-1.050	-1.044	-1.149
$q_{[1,6]}^2$	-1.427	-1.477	-1.474	-1.497	-1.360	-1.301	-1.505
$\mathcal{A}_{FB}^\Xi(\Xi_b \rightarrow \Xi \mu^+ \mu^-) \times 10^3$							
$q_{[0,1,0.98]}^2$	-3.596	-3.606	-3.603	-3.607	-3.609	-3.399	-3.609
$q_{[1,1,2.5]}^2$	-3.558	-3.571	-3.565	-3.572	-3.560	-3.139	-3.567
$q_{[2.5,4]}^2$	-3.505	-3.520	-3.505	-3.516	-3.485	-3.105	-3.502
$q_{[4,6]}^2$	-3.445	-3.461	-3.436	-3.451	-3.401	-3.109	-3.429
$q_{[1,6]}^2$	-3.49	-3.508	-3.492	-3.505	-3.468	-3.117	-3.489

SM, with a decreasing trend observed across all scenarios and channels. For the remaining three q^2 bins, the prediction backwards from all new physics scenarios remain consistent with the SM results. In summary, the new physics scenarios have minimal impact on the longitudinal polarization asymmetry of the baryonic semileptonic decay modes. The transverse polarization asymmetries exhibit a similar pattern to the longitudinal polarization asymmetry.

TABLE VII: Same as Table II, presenting the longitudinal polarization asymmetry observable of $B_1 \rightarrow B_2 \mu^+ \mu^-$ decay modes.

Bins	SM	S - A	S - B	S - C	S - D	S - E	S - F
$\mathcal{F}_L(\Lambda_b \rightarrow \Lambda \mu^+ \mu^-)$							
$q_{[0.1,0.98]}^2$	0.391	0.412	0.359	0.384	0.414	0.402	0.359
$q_{[1.1,2.5]}^2$	0.74	0.66	0.601	0.593	0.66	0.655	0.599
$q_{[2.5,4]}^2$	0.836	0.771	0.774	0.746	0.77	0.775	0.772
$q_{[4,6]}^2$	0.797	0.755	0.78	0.752	0.755	0.759	0.779
$q_{[1,6]}^2$	0.789	0.727	0.717	0.695	0.727	0.728	0.715
$\mathcal{F}_L(\Sigma_b \rightarrow \Sigma \mu^+ \mu^-)$							
$q_{[0.1,0.98]}^2$	0.389	0.395	0.347	0.366	0.391	0.367	0.35
$q_{[1.1,2.5]}^2$	0.597	0.532	0.529	0.505	0.507	0.502	0.539
$q_{[2.5,4]}^2$	0.499	0.47	0.491	0.471	0.444	0.465	0.5
$q_{[4,6]}^2$	0.393	0.381	0.396	0.385	0.363	0.388	0.4
$q_{[1,6]}^2$	0.453	0.431	0.443	0.428	0.408	0.429	0.47
$\mathcal{F}_L(\Xi_b \rightarrow \Xi \mu^+ \mu^-)$							
$q_{[0.1,0.98]}^2$	0.405	0.415	0.356	0.38	0.413	0.406	0.356
$q_{[1.1,2.5]}^2$	0.764	0.68	0.646	0.626	0.671	0.675	0.646
$q_{[2.5,4]}^2$	0.786	0.727	0.747	0.714	0.713	0.732	0.749
$q_{[4,6]}^2$	0.691	0.656	0.686	0.659	0.639	0.67	0.688
$q_{[1,6]}^2$	0.734	0.68	0.688	0.662	0.666	0.686	0.689

IV. SUMMARY AND CONCLUSION

In conclusion, we have conducted a comparative q^2 -binwise analysis of the branching ratios and angular observables for the semileptonic baryonic decay modes $B_1 \rightarrow B_2 \mu^+ \mu^-$, with $B_1 = \Lambda_b, \Sigma_b, \Xi_b$ and $B_2 = \Lambda, \Sigma, \Xi$. This analysis was performed within the Standard Model and across six new physics scenarios involving various combinations of Wilson coefficients: S-A (C_9^{NP}), S-B ($C_9^{\text{NP}} = -C_{10}^{\text{NP}}$), S-C ($C_9^{\text{NP}}, C_{10}^{\text{NP}}$), S-D ($C_9^{\text{NP}}, C_{10}'^{\text{NP}}$), S-E ($C_9^{\text{NP}} = C_9'^{\text{NP}}, C_{10}^{\text{NP}} = C_{10}'^{\text{NP}}$), and S-F ($C_9^{\text{NP}} = -C_{10}^{\text{NP}}, C_9'^{\text{NP}} = C_{10}'^{\text{NP}}$). We derived best-fit values and corresponding 1σ ranges for these coefficients through a global fit to the

TABLE VIII: Same as Table II, presenting the transverse polarization asymmetry observable of $B_1 \rightarrow B_2 \mu^+ \mu^-$ decay modes.

Bins	SM	S - A	S - B	S - C	S - D	S - E	S - F
$\mathcal{F}_T(\Lambda_b \rightarrow \Lambda \mu^+ \mu^-)$							
$q_{[0.1,0.98]}^2$	0.609	0.588	0.641	0.616	0.586	0.508	0.641
$q_{[1.1,2.5]}^2$	0.26	0.34	0.399	0.407	0.44	0.345	0.401
$q_{[2.5,4]}^2$	0.164	0.229	0.226	0.254	0.33	0.225	0.223
$q_{[4,6]}^2$	0.203	0.225	0.22	0.248	0.245	0.241	0.221
$q_{[1,6]}^2$	0.211	0.273	0.283	0.305	0.273	0.272	0.285
$\mathcal{F}_T(\Sigma_b \rightarrow \Sigma \mu^+ \mu^-)$							
$q_{[0.1,0.98]}^2$	0.611	0.605	0.653	0.634	0.609	0.633	0.65
$q_{[1.1,2.5]}^2$	0.403	0.468	0.471	0.495	0.493	0.498	0.461
$q_{[2.5,4]}^2$	0.511	0.53	0.509	0.529	0.666	0.535	0.5
$q_{[4,6]}^2$	0.607	0.619	0.604	0.615	0.637	0.612	0.6
$q_{[1,6]}^2$	0.547	0.569	0.557	0.572	0.592	0.571	0.53
$\mathcal{F}_T(\Xi_b \rightarrow \Xi \mu^+ \mu^-)$							
$q_{[0.1,0.98]}^2$	0.595	0.585	0.644	0.62	0.587	0.594	0.644
$q_{[1.1,2.5]}^2$	0.236	0.32	0.354	0.374	0.329	0.325	0.646
$q_{[2.5,4]}^2$	0.214	0.273	0.253	0.286	0.287	0.268	0.251
$q_{[4,6]}^2$	0.309	0.344	0.314	0.341	0.361	0.33	0.312
$q_{[1,6]}^2$	0.266	0.32	0.312	0.338	0.334	0.314	0.311

$b \rightarrow s \mu^+ \mu^-$ data [44]. Using these constrained coefficients, we made predictions for the branching ratios and angular observables, including forward backward asymmetry, longitudinal polarization asymmetry, and lepton non-universality parameters for the decays $(\Lambda_b, \Sigma_b, \Xi_b) \rightarrow (\Lambda, \Sigma, \Xi) \mu^+ \mu^-$ across five q^2 bins: $[0.1, 0.98]$, $[1.1, 2.5]$, $[2.5, 4]$, $[4, 6]$, and $[1, 6] \text{ GeV}^2$.

Our findings reveal that the branching ratios for the semileptonic baryonic decays $\Lambda_b \rightarrow \Lambda \mu^+ \mu^-$, $\Sigma_b \rightarrow \Sigma \mu^+ \mu^-$, and $\Xi_b \rightarrow \Xi \mu^+ \mu^-$ are consistent with the SM in the $q^2 \in [0.1, 0.98]$ bin. However, significant deviations from the SM are observed in the remaining q^2 intervals,

particularly for new physics scenarios B, C, and F. The lepton non-universality parameters show substantial variations, with scenarios A, D, and E having significant impacts in the first q^2 bin, while B and F align more closely with the SM. Scenarios C, B, and F contribute more prominently in the other q^2 bins. The forward-backward asymmetries (both leptonic and leptonic-hadronic) also exhibit varying degrees of deviation from the SM, with notable shifts in all q^2 regions (except the first q^2 interval) influenced by scenarios B, C, and F. The hadronic forward-backward asymmetries for all the decay modes are found to be within the SM predictions, except for a minor deviation in the $\Sigma_b \rightarrow \Sigma$ mode due to scenario E. Additionally, longitudinal and transverse polarization asymmetries largely align with SM predictions, though minor deviations occur in specific q^2 bins due to new physics scenarios. Overall, these results underscore the potential of semileptonic baryonic decays as sensitive probes of new physics, offering valuable insights and benchmarks for future experimental investigations.

Acknowledgment

AKY extends sincere gratitude to the DST-Inspire Fellowship division, Government of India, for their financial support under ID No. IF210687. MKM acknowledges the financial assistance provided by IoE PDRF from University of Hyderabad.

Appendix A: The angular coefficients (\mathcal{K}_i) for $B_1 \rightarrow B_2$ decays

The angular coefficients \mathcal{K}_i , where $i = 1, 2, 3, 4$, for the decay modes $B_1 \rightarrow B_2 \mu^+ \mu^-$ in terms of the transversity amplitudes are given by [36]

$$\begin{aligned}\mathcal{K}_{1ss} &= \frac{1}{4} (2|A_{||0}^R|^2 + |A_{||1}^R|^2 + 2|A_{\perp 0}^R|^2 + |A_{\perp 1}^R|^2 + R \leftrightarrow L), \\ \mathcal{K}_{1cc} &= \frac{1}{2} (|A_{||1}^R|^2 + |A_{\perp 1}^R|^2 + R \leftrightarrow L), \\ \mathcal{K}_{1c} &= -Re(A_{\perp 1}^R A_{||1}^{*R} - R \leftrightarrow L), \\ \mathcal{K}_{2ss} &= \frac{\alpha_{B_2}}{2} Re(2A_{\perp 0}^R A_{||0}^{*R} + A_{\perp 1}^R A_{||1}^{*R} + R \leftrightarrow L), \\ \mathcal{K}_{2cc} &= \alpha_{B_2} Re(A_{\perp 1}^R A_{||1}^{*R} + A_{\perp 1}^L A_{||1}^{*L}), \\ \mathcal{K}_{2c} &= -\frac{\alpha_{B_2}}{2} Re(|A_{\perp 1}^R|^2 + |A_{||1}^R|^2 - R \leftrightarrow L), \\ \mathcal{K}_{3sc} &= \frac{\alpha_{B_2}}{\sqrt{2}} Im(A_{\perp 1}^R A_{\perp 0}^{*R} - A_{||1}^R A_{||0}^{*R} + R \leftrightarrow L), \\ \mathcal{K}_{3s} &= \frac{\alpha_{B_2}}{\sqrt{2}} Im(A_{\perp 1}^R A_{||0}^{*R} - A_{||1}^R A_{\perp 0}^{*R} - R \leftrightarrow L), \\ \mathcal{K}_{4sc} &= \frac{\alpha_{B_2}}{\sqrt{2}} Re(A_{\perp 1}^R A_{||0}^{*R} - A_{||1}^R A_{\perp 0}^{*R} + R \leftrightarrow L), \\ \mathcal{K}_{4s} &= \frac{\alpha_{B_2}}{\sqrt{2}} Re(A_{\perp 1}^R A_{\perp 0}^{*R} - A_{||1}^R A_{||0}^{*R} - R \leftrightarrow L),\end{aligned}$$

which themselves are expressed in terms of the form factors and Wilson coefficients as follows:

$$\begin{aligned}A_{\perp 1}^{L,R} &= -\sqrt{2}N \left(f_{\perp}^V \sqrt{2s_-} ((C_9^{eff} \mp C_{10}) + (C'_9 \mp C'_{10})) + \frac{2m_b}{q^2} f_{\perp}^T (m_{B_1} + m_{B_2}) \sqrt{2s_-} C_7^{eff} \right), \\ A_{||1}^{L,R} &= \sqrt{2}N \left(f_{\perp}^A \sqrt{2s_+} ((C_9^{eff} \mp C_{10}) - (C'_9 \mp C'_{10})) + \frac{2m_b}{q^2} f_{\perp}^{T5} (m_{B_1} - m_{B_2}) \sqrt{2s_+} C_7^{eff} \right), \\ A_{\perp 0}^{L,R} &= \sqrt{2}N \left(f_0^V (m_{B_1} + m_{B_2}) \sqrt{\frac{s_-}{q^2}} ((C_9^{eff} \mp C_{10}) + (C'_9 \mp C'_{10})) + \frac{2m_b}{q^2} f_0^T \sqrt{q^2 s_-} C_7^{eff} \right), \\ A_{||0}^{L,R} &= -\sqrt{2}N \left(f_0^A (m_{B_1} - m_{B_2}) \sqrt{\frac{s_+}{q^2}} ((C_9^{eff} \mp C_{10}) - (C'_9 \mp C'_{10})) + \frac{2m_b}{q^2} f_0^{T5} \sqrt{q^2 s_+} C_7^{eff} \right),\end{aligned}$$

where, $s_{\pm} = (m_{B_1} \pm m_{B_2})^2 - q^2$ and the normalization constant N is represented as

$$N = \left[\frac{G_F^2 |V_{tb} V_{ts}^*|^2 \alpha_e^2}{3.2^{11} m_{B_1}^3 \pi^5} q^2 \lambda^{1/2}(m_{B_1}^2, m_{B_2}^2, q^2) \beta_l \right]^{1/2},$$

with

$$\beta_l = \sqrt{1 - \frac{4m_l^2}{q^2}}, \text{ and } \lambda(m_{B_1}^2, m_{B_2}^2, q^2) = m_{B_1}^4 + m_{B_2}^4 + q^4 - 2(m_{B_1}^2 m_{B_2}^2 + m_{B_2}^2 q^2 + q^2 m_{B_1}^2).$$

Appendix B: Form factors of the $B_1 \rightarrow B_2 l^+ l^-$ modes

a. $\Xi_b \rightarrow \Xi$ and $\Sigma_b \rightarrow \Sigma$ (Light cone QCD sum rule)

The expression for the form factors of $\Xi_b \rightarrow \Xi$ [29] and $\Sigma_b \rightarrow \Sigma$ [28] is given by

$$F_i(q^2) = \frac{a}{(1 - \frac{q^2}{m_{fit}^2})} + \frac{b}{(1 - \frac{q^2}{m_{fit}^2})^2}, \quad (\text{B1})$$

where, $F = f, g$, $i = 1, 2, 3$. The input values of a , b , m_{fit} are presented in Table IX and X.

TABLE IX: Parameters used in the form factors for $\Xi_b \rightarrow \Xi \ell^+ \ell^-$ transition [29].

	a	b	m_{fit}		a	b	m_{fit}
f_1	0.166	-0.024	5.35	f_1^T	0.127	-0.129	5.10
f_2	0.028	-0.048	5.31	f_2^T	0.072	0.085	5.40
f_3	-0.004	-0.006	5.37	f_3^T	-0.003	0.049	5.23
g_1	0.106	0.054	5.24	g_1^T	0.288	-0.312	4.80
g_2	-0.005	-0.004	5.28	g_2^T	0.036	0.119	4.70
g_3	0.003	-0.006	4.70	g_3^T	0.024	-0.095	5.33

b. $\Lambda_b \rightarrow \Lambda$ (Lattice QCD)

The form factors for $\Lambda_b \rightarrow \Lambda$ in lattice QCD [34] are given by

$$f(q^2) = \frac{1}{1 - q^2/(m_{\text{pole}}^f)^2} [a_0^f + a_1^f z(q^2) + a_2^f [z(q^2)]^2]. \quad (\text{B2})$$

The values and uncertainties of the parameters a_0^f , a_1^f and a_2^f from the nominal fit are given in Table XI.

TABLE X: Parameters used in the form factors for $\Sigma_b \rightarrow \Sigma \ell^+ \ell^-$ decay [28].

	a	b	m_{fit}		a	b	m_{fit}
f_1	$-(0.035 \pm 0.006)$	0.130 ± 0.023	5.1 ± 1.0	f_1^T	1.0 ± 0.0	$-(1.0 \pm 0.0)$	5.4 ± 1.1
f_2	0.026 ± 0.006	$-(0.081 \pm 0.018)$	5.2 ± 1.0	f_2^T	$-(0.290 \pm 0.089)$	0.421 ± 0.129	5.4 ± 1.1
f_3	0.013 ± 0.004	$-(0.065 \pm 0.020)$	5.3 ± 1.1	f_3^T	$-(0.240 \pm 0.071)$	0.412 ± 0.122	5.4 ± 1.1
g_1	$-(0.031 \pm 0.008)$	0.151 ± 0.038	5.3 ± 1.1	g_1^T	0.450 ± 0.135	$-(0.460 \pm 0.138)$	5.4 ± 1.1
g_2	0.015 ± 0.005	$-(0.040 \pm 0.013)$	5.3 ± 1.1	g_2^T	0.031 ± 0.009	0.055 ± 0.015	5.4 ± 1.1
g_3	0.012 ± 0.003	$-(0.047 \pm 0.012)$	5.4 ± 1.1	g_3^T	$-(0.011 \pm 0.003)$	$-(0.180 \pm 0.057)$	5.4 ± 1.1

 TABLE XI: Parameters used in the form factor for $\Lambda_b \rightarrow \Lambda \ell^+ \ell^-$ transition [34].

Parameter	Value	Parameter	Value
a_0^{f+}	0.4229 ± 0.0274	$a_2^{g_0}$	1.1490 ± 1.0327
a_1^{f+}	-1.3728 ± 0.3068	$a_1^{g_+}$	-1.3607 ± 0.2949
a_2^{f+}	1.7972 ± 1.1506	$a_2^{g_+}$	2.4621 ± 1.3711
$a_0^{f_0}$	0.3604 ± 0.0277	a_0^{h+}	0.4753 ± 0.0423
$a_1^{f_0}$	-0.9248 ± 0.3453	a_1^{h+}	-0.8840 ± 0.3997
$a_2^{f_0}$	0.9861 ± 1.1988	a_2^{h+}	-0.8190 ± 1.6760
$a_0^{f_\perp}$	0.5148 ± 0.0353	$a_0^{h_\perp}$	0.3745 ± 0.0313
$a_1^{f_\perp}$	-1.4781 ± 0.4030	$a_1^{h_\perp}$	-0.9439 ± 0.2766
$a_2^{f_\perp}$	1.2496 ± 1.6396	$a_2^{h_\perp}$	1.1606 ± 1.0757
$a_0^{g_\perp, g_+}$	0.3522 ± 0.0205	$a_0^{\tilde{h}_\perp, \tilde{h}_+}$	0.3256 ± 0.0248
$a_1^{g_+}$	-1.2968 ± 0.2732	$a_1^{\tilde{h}_+}$	-0.9603 ± 0.2303
$a_2^{g_+}$	2.7106 ± 1.0665	$a_2^{\tilde{h}_+}$	2.9780 ± 1.0041
$a_0^{g_0}$	0.4059 ± 0.0267	$a_1^{\tilde{h}_\perp}$	-0.9634 ± 0.2268
$a_1^{g_0}$	-1.1622 ± 0.2929	$a_2^{\tilde{h}_\perp}$	2.4782 ± 0.9549

-
- [1] R. Aaij *et al.* (LHCb), JHEP **08**, 055 (2017), arXiv:1705.05802 [hep-ex].
- [2] S. Wehle *et al.* (Belle), Phys. Rev. Lett. **118**, 111801 (2017), arXiv:1612.05014 [hep-ex].

- [3] A. Hayrapetyan *et al.* (CMS), *Rept. Prog. Phys.* **87**, 077802 (2024), arXiv:2401.07090 [hep-ex].
- [4] G. Hiller and F. Kruger, *Phys. Rev. D* **69**, 074020 (2004), arXiv:hep-ph/0310219 .
- [5] R. Aaij *et al.* (LHCb), *Phys. Rev. Lett.* **131**, 051803 (2023), arXiv:2212.09152 [hep-ex] .
- [6] R. Aaij *et al.* (LHCb), *Phys. Rev. D* **108**, 032002 (2023), arXiv:2212.09153 [hep-ex] .
- [7] R. Aaij *et al.* (LHCb), *Phys. Rev. Lett.* **111**, 191801 (2013), arXiv:1308.1707 [hep-ex] .
- [8] R. Aaij *et al.* (LHCb), *JHEP* **02**, 104 (2016), arXiv:1512.04442 [hep-ex] .
- [9] M. Aaboud *et al.* (ATLAS), *JHEP* **10**, 047 (2018), arXiv:1805.04000 [hep-ex] .
- [10] R. Aaij *et al.* (LHCb), *Phys. Rev. Lett.* **127**, 151801 (2021), arXiv:2105.14007 [hep-ex] .
- [11] R. Aaij *et al.* (LHCb), *JHEP* **11**, 043 (2021), arXiv:2107.13428 [hep-ex] .
- [12] R. Aaij *et al.* (LHCb), *JHEP* **09**, 179 (2015), arXiv:1506.08777 [hep-ex] .
- [13] R. Aaij *et al.* (LHCb), *Phys. Rev. Lett.* **128**, 191802 (2022), arXiv:2110.09501 [hep-ex] .
- [14] R. Aaij *et al.* (LHCb), *JHEP* **12**, 081 (2020), arXiv:2010.06011 [hep-ex] .
- [15] R. Aaij *et al.* (LHCb), *Phys. Rev. Lett.* **125**, 011802 (2020), arXiv:2003.04831 [hep-ex] .
- [16] R. Aaij *et al.* (LHCb), *Phys. Rev. Lett.* **123**, 081802 (2019), arXiv:1905.06284 [hep-ex] .
- [17] R. Aaij *et al.* (LHCb), *JHEP* **06**, 133 (2014), arXiv:1403.8044 [hep-ex] .
- [18] *Angular analysis of the $B^0 \rightarrow K^{*0}(892)\mu^+\mu^-$ decay at $\sqrt{s} = 13$ TeV*, Tech. Rep. (CERN, Geneva, 2024).
- [19] J. P. Lees *et al.* (BaBar), *Phys. Rev. D* **86**, 032012 (2012), arXiv:1204.3933 [hep-ex] .
- [20] D. e. a. Dutta, (2015).
- [21] F. Mahmoudi and Y. Monceaux, *Symmetry* **16**, 1006 (2024), arXiv:2408.03235 [hep-ph] .
- [22] G. Buchalla, A. J. Buras, and M. E. Lautenbacher, *Rev. Mod. Phys.* **68**, 1125 (1996), arXiv:hep-ph/9512380 .
- [23] T. Aaltonen *et al.* (CDF), *Phys. Rev. Lett.* **107**, 201802 (2011), arXiv:1107.3753 [hep-ex] .
- [24] R. Aaij *et al.* (LHCb), *Phys. Lett. B* **725**, 25 (2013), arXiv:1306.2577 [hep-ex] .
- [25] R. Aaij *et al.* (LHCb), *JHEP* **06**, 115 (2015), [Erratum: *JHEP* 09, 145 (2018)], arXiv:1503.07138 [hep-ex] .
- [26] R. Aaij *et al.* (LHCb), *Phys. Rev. Lett.* **120**, 221803 (2018), arXiv:1712.08606 [hep-ex] .
- [27] R. Aaij *et al.* (LHCb), *JHEP* **01**, 069 (2022), arXiv:2108.07678 [hep-ex] .
- [28] N. Katirci and K. Azizi, *J. Phys. G* **40**, 085005 (2013), arXiv:1207.4053 [hep-ph] .
- [29] K. Azizi, Y. Sarac, and H. Sundu, *Eur. Phys. J. A* **48**, 2 (2012), arXiv:1107.5925 [hep-ph] .

- [30] T. M. Aliev, K. Azizi, and M. Savci, *Phys. Rev. D* **81**, 056006 (2010), arXiv:1001.0227 [hep-ph]
- [31] K. Azizi, S. Kartal, A. T. Olgun, and Z. Tavukoglu, *Phys. Rev. D* **88**, 075007 (2013), arXiv:1307.3101 [hep-ph].
- [32] T. Gutsche, M. A. Ivanov, J. G. Korner, V. E. Lyubovitskij, and P. Santorelli, *Phys. Rev. D* **87**, 074031 (2013), arXiv:1301.3737 [hep-ph].
- [33] P. Böer, T. Feldmann, and D. van Dyk, *JHEP* **01**, 155 (2015), arXiv:1410.2115 [hep-ph].
- [34] W. Detmold and S. Meinel, *Phys. Rev. D* **93**, 074501 (2016), arXiv:1602.01399 [hep-lat].
- [35] R. N. Faustov and V. O. Galkin, *Phys. Rev. D* **94**, 073008 (2016), arXiv:1609.00199 [hep-ph].
- [36] D. Das, *JHEP* **07**, 063 (2018), arXiv:1804.08527 [hep-ph].
- [37] D. Das, J. Das, G. Kumar, and N. Sahoo, *Phys. Rev. D* **108**, 015001 (2023), arXiv:2211.09065 [hep-ph].
- [38] S. Sahoo and R. Mohanta, *New J. Phys.* **18**, 093051 (2016), arXiv:1607.04449 [hep-ph].
- [39] R. Mohanta and A. K. Giri, *Phys. Rev. D* **82**, 094022 (2010), arXiv:1010.1152 [hep-ph].
- [40] G. Kumar and N. Mahajan, (2015), arXiv:1511.00935 [hep-ph].
- [41] W.-H. Tan, H.-M. Yang, and H.-X. Chen, *Eur. Phys. J. C* **84**, 382 (2024), arXiv:2311.18380 [hep-ph].
- [42] R.-M. Wang, Y.-G. Xu, C. Hua, and X.-D. Cheng, *Phys. Rev. D* **103**, 013007 (2021), arXiv:2101.02421 [hep-ph].
- [43] F. Erben, V. Gülpers, M. T. Hansen, R. Hodgson, and A. Portelli, *JHEP* **04**, 108 (2023), arXiv:2209.15460 [hep-lat].
- [44] M. K. Mohapatra, A. K. Yadav, and S. Sahoo, (2024), arXiv:2409.01269 [hep-ph].
- [45] A. Ali, P. Ball, L. T. Handoko, and G. Hiller, *Phys. Rev. D* **61**, 074024 (2000), arXiv:hep-ph/9910221 .
- [46] S. Navas *et al.* (Particle Data Group), *Phys. Rev. D* **110**, 030001 (2024).
- [47] A. Ray, S. Sahoo, and R. Mohanta, *Phys. Rev. D* **99**, 015015 (2019).